Growth of zirconium silicide nanostructures on vicinal and flat Si(111)-7 × 7 surfaces

2008 J. Phys.: Condens. Matter 20 225015

(http://iopscience.iop.org/0953-8984/20/22/225015)

J. Phys.: Condens. Matter **20** (2008) 225015 (5pp) doi:10.1088/0953-8984/20/22/225015

Growth of zirconium silicide nanostructures on vicinal and flat Si(111)-7 × 7 surfaces

Bin Lu[1,2,3], **Wende Xiao**[1], **Sunil Singh Kushvaha**[1], **Pimo He**[2] and **Xue-Sen Wang**[1,3]

[1] Department of Physics, National University of Singapore, 2 Science Drive 3, Singapore 117542, Singapore
[2] Department of Physics, Zhejiang University, Hangzhou 310027, People's Republic of China

E-mail: binlu@zju.edu.cn and phywxs@nus.edu.sg

Received 8 November 2007, in final form 16 April 2008
Published 15 May 2008
Online at stacks.iop.org/JPhysCM/20/225015

Abstract

Using *in situ* scanning tunneling microscopy and low-energy electron diffraction, we performed investigations on the growth of zirconium silicide on vicinal and flat Si(111)-7 × 7 surfaces. In the case of a solid-phase reaction, submonolayer zirconium deposition onto vicinal Si followed by successive annealing results in the formation of zirconium silicide nanostructures, which are distributed randomly on the surface. These nanostructures evolved into rod-shaped islands with axes running along the substrate $\langle\bar{1}10\rangle$ directions at the late stage of the coarsening process. When 2–3 monolayers of Zr are deposited on Si at 520 °C, an extended network with rod-like silicide domains was developed, which is controlled by the elastic strain-relief mechanism. The atomic structures of these silicide features were identified and they are considered to adopt C49 $ZrSi_2$. The reaction and growth on a flat surface with less Zr coverage at higher temperatures led to the formation of longer and narrower nanowires. The relations between the variety of nanostructures and the different growth conditions are addressed.

(Some figures in this article are in colour only in the electronic version)

1. Introduction

The formation of low-dimensional nanostructures on semiconductor surfaces via metal deposition and growth has attracted much interest in recent years [1–6]. These nanostructures exhibit novel electronic properties with quantum effects caused by electron confinement [7], and are hence potentially useful in future generation of electronic and optoelectronic devices. There are various methods for fabrication of such nanostructures. Among them, self-assembly, in which the desired nanostructures are spontaneously formed during heteroepitaxy, is a low-cost, parallel approach for industrial applications.

Metal silicides such as $MoSi_2$ and $TiSi_2$ are of interest as interconnections and contacts in sub-100 nm gate MOSFET devices [8–12]. However, $MoSi_2$ has a high electric resistivity. Although $TiSi_2$ exhibits a quite low resistivity in the C54 phase (face-centered orthorhombic), it suffers from having a metastable low-temperature phase with four times higher resistivity. The metastable phase of $TiSi_2$ has an orthorhombic-base-centered lattice structure, i.e. $ZrSi_2$ structure (C49), and the phase transition occurs at around 650 °C [11].

Since zirconium is in the same group (IVa) in the periodic table as Ti, Zr silicide is expected to have similar physical and chemical characteristics as Ti silicide. The Zr silicide formed by the thin film reaction with Zr deposited on silicon also exhibits a relatively low resistivity (35–40 $\mu\Omega$ cm) and high thermal stability [13, 14]. A Schottky barrier height of 0.55 eV, about half of the Si bandgap, was reported for $ZrSi_2$ on n-type Si [15]. In addition, one advantage of $ZrSi_2$ over $TiSi_2$ is that it is stable in the C49 phase [16, 17]. Structurally, $ZrSi_2$ has a peculiar pseudolamellar crystal structure with lattice parameters of $a = 0.369$ nm, $b = 1.47$ nm, and $c = 0.366$ nm [18]. In addition, Zr oxide is a promising high-k dielectric material [19], making $ZrSi_2$ highly compatible.

[3] Authors to whom any correspondence should be addressed.

In this paper, we report on our experimental investigations of Zr silicide nanostructural growth on Si(111) surfaces. *In situ* scanning tunneling microscopy (STM) was employed to study Zr deposition and the solid-phase reaction as well as the evolution of Zr silicide nanostructures on flat and vicinal Si(111)-7 × 7. The detailed correlation between the evolution of Zr silicide nanostructures and the growth conditions is explored.

2. Experimental details

The experiments were carried out in an Omicron ultra-high vacuum (UHV) system (base pressure ∼1 × 10^{-10} mbar) equipped with STM, four-grid low-energy electron diffraction (LEED) and Auger electron spectroscopy (AES) apparatus. An electron beam bombardment heater was used for sample annealing and a resistive-heating source was used for Zr evaporation. Si(111) samples cut from commercial wafers (n-type, $\rho \sim 10\ \mu\Omega$ cm) were mounted on pre-degassed refractory metal holders. The Si(111)-7 × 7 surface was prepared by degassing the sample at low temperature for several hours, followed by flashing to 1200 °C for 1 min with the chamber pressure below 1 × 10^{-9} mbar. The sample cleanliness was verified by STM, LEED and AES.

Zr was deposited onto the substrate at a deposition rate of the order of 0.1 ML min^{-1} (1 ML = 7.8 × 10^{14} Zr atoms cm^{-2}, corresponding to one atom per Si(111)-1 × 1 unit cell) with the substrate temperature ranging from room temperature (RT) to 800 °C. For the solid-phase reaction, Zr was deposited onto a vicinal Si(111)-7 × 7 surface at RT, and the sample was annealed *in situ* for 20 min after each deposition. The reaction and growth of Zr on a flat Si(111)-7 × 7 surface was also done by Zr deposition on a heated substrate. All the STM measurements were performed in a constant-current mode at RT. LEED and AES were also used to check the deposition amount and surface reconstruction.

3. Results and discussion

3.1. Solid-phase reaction and Zr silicide nanostructural growth on vicinal Si(111)

Deposition of 0.4 ML Zr at low temperature (without intentional heating, the sample was at ∼80 °C during Zr deposition due to irradiation from the evaporation source) on a vicinal Si(111)-7 × 7 results in small clusters randomly distributed on the surface, while 7 × 7 reconstruction is still visible between the clusters (not shown). These clusters are ∼1–2 nm in diameter and ∼0.3 nm in height. After annealing below 300 °C, no evidence of a reaction between the deposited Zr and Si substrate was found. The reaction begins as the sample is annealed at 300–350 °C. The clusters aggregate and increase in size. As shown in figure 1(a), the clusters typically are 2–3 nm in diameter with irregular shape. Meanwhile, significant destruction of 7 × 7 was observed, and this is believed to be due to the migration of Si atoms for the formation of amorphous Zr silicide. These results indicate the initiation of Zr silicidation at low Zr coverage in this

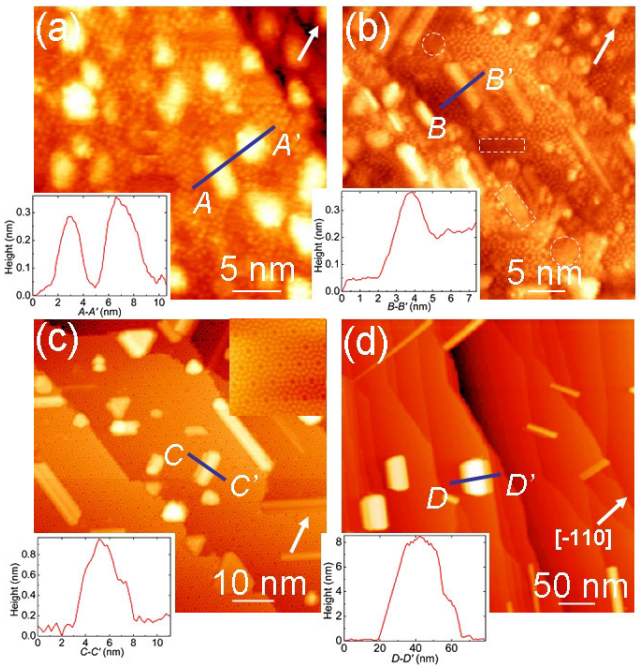

Figure 1. (a) STM image (taken with $V_s = 2.0$ V, $I = 1$ nA) after 0.4 ML Zr deposited on a vicinal Si(111)-7 × 7 surface at RT followed by annealing at 300–350 °C for 20 min, showing the initial reaction of Zr atoms with substrate. The region 7 × 7 in area between the clusters was destroyed. The morphology evolution of the surface and Zr silicide nanostructures after successive annealing at (b) 520 °C, (c) 630 °C and (d) 840 °C for 20 min each. Insets are line profiles across typical nanostructures formed after annealing at different temperatures. Depressions and/or pits in (b) are indicated by dashed circles/rectangles. The top-right inset in (c) shows the 7 × 7 on the surface between silicide islands.

temperature range, similar to the previous report by Yamauchi *et al* on the Zr/Si(001) growth study [20]. However, the clusters are amorphous and the silicidation process is incomplete.

Further annealing the sample at 520–1020 °C leads to the formation of three-dimensional (3D) crystalline nanostructures. The density of these nanostructures decreases while their average height and width increase as shown in the series of STM images displayed in figures 1(b)–(d).

After annealing the sample at 520 °C for 20 min, the STM image (figure 1(b)) reveals the formation of silicide nanocrystallites, with some having a rod shape. Depressions and pits can be seen next to some nanocrystallites, indicating that more Si is supplied for the silicide formation from the terraces. This observation is also compatible with the previously reported solid-phase reaction in the Zr/Si(001) system [20], where only a crystalline $ZrSi_2$ layer was formed at the interface by annealing the sample above 560 °C. Other silicides, such as ZrSi, were not detected. This is reasonable since in a Si-rich environment, the Si-rich Zr silicide phase forms preferably if Si atoms can diffuse rapidly. The inset in figure 1(b) shows a profile along the line B–B'. The heights of the nanostructures are typically about 0.25–0.5 nm. Some nanostructures are partially embedded in the substrate.

With increasing annealing temperature to 630 °C, the density of silicide islands decreases, while their average size

increases significantly (see figure 1(c)). The large islands grow and coarsen by consuming the small ones. The islands mostly take a short rod or triangular shape, besides some irregular ones. As illustrated in the top-right inset in figure 1(c), the bare areas between the islands are well-ordered Si(111)-7 × 7 surfaces, which are also confirmed by LEED observation. Thus, 630 °C is sufficient to activate surface diffusion that results in (i) the epitaxial growth of zirconium silicide crystallites on Si(111) and (ii) the restoration of Si(111)-7 × 7 in bare areas. We believe that all Zr atoms deposited have gathered to form silicide crystallites, because the annealing temperature is too low for Zr atoms to re-evaporate from the surface. There is also clear evidence of step edge pinning by silicide islands. The supply of Si atoms for silicide island growth makes the steps more rugged than those on the surface prior to Zr deposition. The elongated or triangular Zr silicide crystallites are oriented with their sides running along the three equivalent $\langle\bar{1}10\rangle$ directions. Zr silicide islands are randomly distributed on the surface, and the nucleation and growth of these islands occur both at the steps and on the terraces.

A further annealing at 840 °C accelerates the coarsening of Zr silicide islands. The island density decreases dramatically (figure 1(d)), leaving much of the bare surface with well-ordered 7 × 7 reconstruction. Now, the islands are mostly nanorods and rectangular crystallites, with triangular ones rarely found. Tersoff and Tromp [21] pointed out that a strained epitaxial island can effectively reduce the elastic energy by growing in a rod shape. This is probably a major driving force for the Zr silicide to form nanorods here. At this stage, the islands are still aligned along the $\langle\bar{1}10\rangle$ directions on Si(111). The maximum length of silicide rods is ∼100 nm, and they can even grow across substrate steps.

The morphology of a typical elongated island is presented in figures 2(a) and (b). On the island surface, parallel strips separated by trenches were observed, indicating the formation of dislocations. A similar structure was also observed in the systems of Dy/Si(001) [22] and Sc/Si(111) [23]. As shown in detail in figure 2(b), the island surface is characterized with quasi-periodic atomic protrusions in a dentate arrangement along the strips. In addition, the features of the islands are oriented in a well-defined way with respect to the substrate, indicating epitaxial growth in the present growth conditions. The measured periodicity in the perpendicular $\langle 11\bar{2}\rangle$ direction is 2.50 ± 0.10 nm, which corresponds to about 7.5 times of the substrate periodicity. As described by Bourret *et al* [18], the C49 phase $ZrSi_2$ crystalline film can be heavily faulted in the (010) plane. However, it is hard to examine the internal lattice with STM measurements, and thus we adopt the same structure as that in its crystalline film. Based on the STM observations, the surface of the islands looks like the (100) or (100) plane of Zr disilicide with $\langle b\rangle$ perpendicular to the trenches. The epitaxial growth of Zr silicide involves strain because of lattice mismatch between the silicide and the substrate. As can be seen in figure 1(d), the rectangular islands have typical height of several nm and width of several tens of nm. With such a large size, strain relief is difficult except at the edges. The formation of trenches could lead to partial strain relief and lower the total system energy, i.e. their formation thus could be energetically favored.

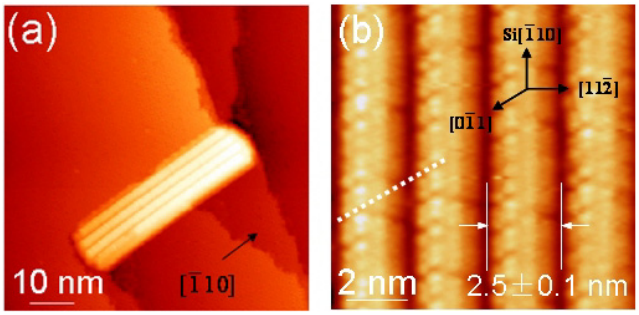

Figure 2. (a) STM image of an elongated silicide island along the step edge, showing a strip structure on the top surface. (b) High-resolution STM image ($V_s = 1.8$ V, $I = 0.8$ nA) showing a 'dentate' structure of the island surface. As indicated by the white dash line, the 'teeth' are aligned parallel to [$0\bar{1}1$] of Si. The stripes with a period ∼2.5 nm can be identified with a scan in the Si [$11\bar{2}$] direction (a scan angle rotated by 29°).

Further thermal treatment of the sample to above 1000 °C results in even larger islands that could only be found by scanning a large area (density $<10^8$ cm^{-2}). These large islands are several tens of nm in height and are difficult to image with STM. The coarsening of the islands takes place probably in a process in which atoms detach themselves from smaller islands and are preferentially absorbed by larger ones after diffusing through the adatom sea. The direct coalescence of silicide islands can be ruled out due to an extremely low mobility of an entire silicide island on the surface. This is because of the strong epitaxial bonding between the silicides and substrate. Coalescence events without cluster diffusion are very rare because of the low island density in the late stages of the coarsening process [24].

3.2. Zr deposition and silicide growth at elevated temperatures

In order to avoid the influence of steps, a flat Si(111) instead of a vicinal one was used. Figure 3(a) shows the STM image with an extended network structure of Zr silicide, taken on a sample prepared by depositing ∼2.5 ML Zr with a flux of ∼0.1 ML min^{-1} on Si(111) held at 520 °C. Similar to the previous solid-phase reaction growth, the rod-like structures are all along the three equivalent $\langle\bar{1}10\rangle$ directions with typical lengths of 20–70 nm. Similar nanorod networks have also been reported for Sc silicide [23] and Er silicide [25] on Si(111). As we proposed above, the rod-like structures are considered to result from an anisotropic strain relaxation that favors long thin structures aligned in the direction with a small mismatch. The mismatch of the Si period along $\langle\bar{1}10\rangle$ (i.e. 0.384 nm) is 3.9% with the lattice constant $\langle a\rangle = 0.369$ nm of $ZrSi_2$ and is 4.7% with $\langle c\rangle = 0.366$. The strained epitaxial growth in these directions is possible within a limited structural thickness. In the perpendicular $\langle 11\bar{2}\rangle$ directions, the epitaxial growth is restrained due to the high possibility of a $\pi/2$-rotation twin around the b axis in the silicide [18].

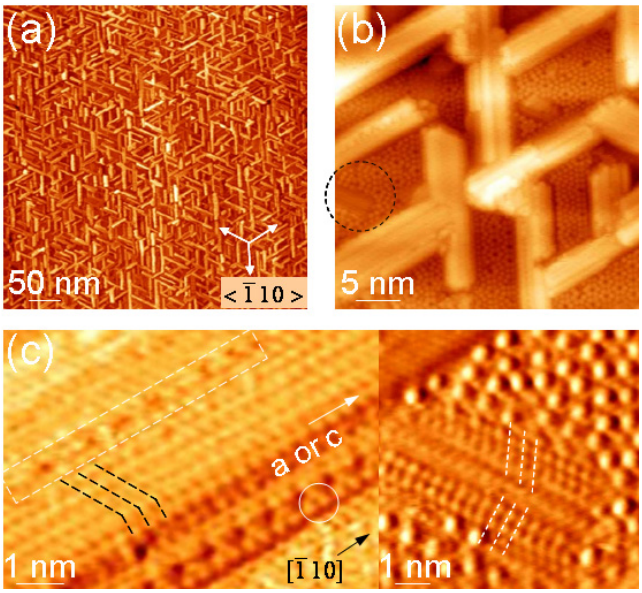

Figure 3. (a) STM image of an extended network of Zr silicide nanorods grown with 2.5 ML Zr deposited on Si(111) at ∼520 °C. (b) A zoom-in STM image ($V_s = 1.9$ V, $I = 0.9$ nA) showing the areas between the rods with 7 × 7 visible. A silicide domain within the 7 × 7 area is observed in the dashed-line circle. (c) Contrast-enhanced atomic resolution images ($V_s = 1.4$ V, $I = 0.9$ nA) of the silicide domain structures. The left image is on a protruded rod and the right one is from the dashed-line circle in (b). The misalignments labeled by the dashed lines as well as the stacking displacement boundary (labeled by the dashed rectangle) can be observed. The paired structure at the side of the silicide domain is marked by a circle.

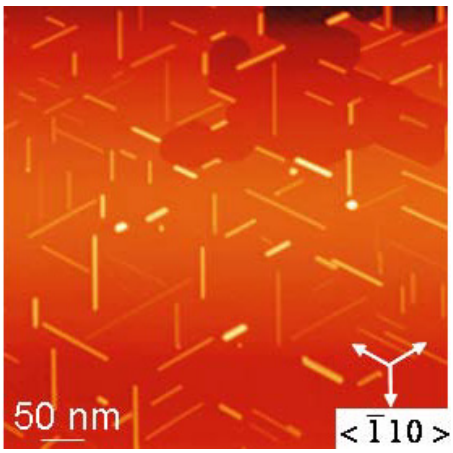

Figure 4. STM image of Zr silicide nanorods grown with 0.16 ML of Zr deposited on flat Si(111) at 790 °C.

The enlarged STM image shown in figure 3(b) provides more detail. Pits and distortions were sometimes observed in the areas adjacent to the silicide structures. Formation of pits or distortions could relieve the stress between them and lower the system energy. The substrate 7 × 7 remains visible between silicide areas. The atomic structures of the silicide domains are presented in figure 3(c). The left panel shows the structures on a protruding silicide rod and the right panel is the embedded silicide domain in the dashed-line circle in figure 3(b). In the left panel, the hexagon-like lattice with a period of 0.375 ± 0.01 nm should be along the *a* axis (or *c* axis) of $ZrSi_2$. Furthermore, the misalignments marked with dashed lines can be seen for the silicide domains. The observed features are compatible with the previous electron diffraction observations [18] and therefore are confirmed to be the (100) or the (001) plane of $ZrSi_2$. The disordered area in the dashed-line rectangle in the left panel may result from the $\pi/2$-rotation around the *b* axis or other displacement in the (010) plane of $ZrSi_2$ [18]. The embedded silicide domain in the right panel also shows the misalignments. It should be pointed out that the same tunneling bias and current were used for imaging these two areas while the tip condition varied. The paired structures at the side position marked with a circle in figure 3(c) appeared as a monomer with other imaging conditions.

The reason why the relatively broad island with trenches is not observed here is believed to be mainly due to different temperatures used at the growth stage in the two types of samples. Deposition at 520 °C, although it is even lower than that used for annealing in the solid-state reaction growth to get the sample shown in figure 1(c), is high enough for Zr and Si atom migration to facilitate nanorod growth. When clusters and small silicide islands are formed at a lower temperature, it is rather difficult for them to migrate for forming elongated rods even annealed later at a higher temperature, so relatively broad islands are common. For such broad silicide islands, trenched structures help to reduce elastic energy. The self-assembly growth of thin rod-like silicide is more effective for elastic strain energy relief, without the need for forming trenches. The further elongation of the rods is obstructed by other rods due to their high density on the sample shown in figure 3(a). In other words, it appears that lower Zr coverage and deposition flux at a higher substrate temperature should increase the average rod length.

To verify the above observation, we deposited 0.16 ML Zr on a Si(111)-7 × 7 substrate at 790 °C with a flux of 0.06 ML min^{-1}. An STM image of the resulting sample is shown in figure 4. Comparing figures 4 and 3(a), it is obvious that a lower coverage and a higher temperature indeed lead to the growth of longer Zr silicide nanorods with an average width of 3.2 nm. The self-assembly of long nanorods requires an extremely high anisotropy in the growth rate. That is, atoms preferentially attach to the ends of nanorods, whereas little nucleation and growth occur on the sidewalls. Such a high-growth anisotropy requires large differences of atomic sticking and diffusion rates on different facets of the growing crystalline objects [26]. In our case, the landing sites of Zr atoms on the Si surface should be random and rather uniform. Zr atoms diffuse not only to the ends but also to the sidewalls of the rods. For those Zr atoms landed on or diffused to the relatively inert sidewalls, at a high temperature and low deposition flux, the fast atomic diffusion rate makes the nucleation of stable nuclei basically impossible, so they diffuse rapidly to the ends, resulting in the further elongation of the rods.

4. Conclusions

Various Zr silicide nanostructures have been fabricated on vicinal and flat Si(111) surfaces after Zr deposition and annealing at different temperatures. Zr deposition at RT followed by annealing at higher temperatures yields triangular ($T \leqslant 630\,^{\circ}$C), rectangular ($T \geqslant 520\,^{\circ}$C) and rod-shaped silicide islands. 2.5 ML Zr deposition at 520 °C with a high flux leads to a high-density network of short silicide nanorods, while 0.16 ML Zr deposition at 790 °C with a low flux results in low density but long silicide nanorods. Strain relief is the main driving force for the self-assembly of rectangular Zr disilicide islands with trenches and nanorods. A higher substrate temperature during Zr deposition with a relatively low flux favors the formation of longer nanorods, due to an enhanced growth anisotropy as a result of high atomic mobility and negligible nucleation probability on the sidewalls of the nanorods. These results illustrate that Zr silicide nanostructures with selected shape and other geometry parameters can be fabricated by proper control of growth conditions.

Acknowledgments

This work was partially supported by research grants from the National University of Singapore (Grant R-144-000-184-112) and the Science and Engineering Research Council of Singapore (Grant R-144-000-088-305).

References

[1] Nogami J, Liu B Z, Katkov M V, Ohbuchi C and Birge N O 2001 *Phys. Rev.* B **63** 233305
[2] Fitting L, Zeman M C, Yang W-C and Nemanich R J 2003 *J. Appl. Phys.* **93** 4180
[3] He Z, Stevens M, Smith D J and Bennett P A 2003 *Surf. Sci.* **524** 148
[4] Li S C, Jia J F, Dou R F, Xue Q K, Batyrev I G and Zhang S B 2004 *Phys. Rev. Lett.* **93** 116103
[5] Negishi R, Mochizuki I and Shigeta Y 2006 *Surf. Sci.* **600** 1125
[6] Zhou W, Zhu Y, Ji T, Hou X Y and Cai Q 2006 *Nanotechnology* **17** 852
[7] Barke I and Hövel H 2003 *Phys. Rev. Lett.* **90** 166801
[8] Murarka S P 1980 *J. Vac. Sci. Technol.* **17** 775
[9] Murarka S P and Fraser D B 1980 *J. Appl. Phys.* **51** 350
[10] d'Heurle F M 1998 *J. Mater. Res.* **3** 167
[11] Jeon H, Sukow C A, Honecutt J W, Rozgonyi G A and Nemanich R J 1992 *J. Appl. Phys.* **71** 4269
[12] Maex K 1993 *Mater. Sci. Eng.* R **11** 53
[13] Sukow C A and Nemanich R J 1994 *J. Mater. Res.* **9** 1214
[14] Jeon H and Kim S 1998 *Japan. J. Appl. Phys.* **37** 4747
[15] Lau S S, Chu W K, Mayer J W and Tu K N 1974 *Thin Solid Films* **23** 205
[16] Setton M and Van der Spiegel J 1991 *J. Appl. Phys.* **70** 193
[17] Lin J H, Hsieh W Y and Chen L J 1996 *J. Appl. Phys.* **79** 9123
[18] Bourret A, d'Heurie F M, Le Goues F K and Charai A 1990 *J. Appl. Phys.* **67** 241
[19] Zhao X, Ceresoli D and Vanderbilt D 2005 *Phys. Rev.* B **71** 085107
[20] Yamauchi T, Zaima S, Mizuno K, Kitmura H, Koide Y and Yasuda Y 1991 *J. Appl. Phys.* **69** 7050
[21] Tersoff J and Tromp R M 1993 *Phys. Rev. Lett.* **70** 2782–5
[22] Preinesberger C, Becker S K, Vandré S, Kalka T and Dähne D 2002 *J. Appl. Phys.* **91** 1695
[23] Nörenberg C, Moram M A and Dobson P J 2006 *Surf. Sci.* **600** 4126
[24] Krause M R, Stollenwerk A, Licurse M and LaBella V P 2006 *J. Vac. Sci. Technol.* A **24** 1480
[25] Wetzel P, Pirri C, Gewinner G, Pelletier S, Roge P and Palmino F 1997 *Phys. Rev.* B **56** 9819
[26] Xia Y, Yang P, Sun Y, Wu Y, Mayers B, Gates B, Yin Y, Kim F and Yan H 2003 *Adv. Mater.* **15** 353